Korean Chem. Eng. Res., 57(2), 289-300 (2019)
https://doi.org/10.9713/kcer.2019.57.2.289
PISSN 0304-128X, EISSN 2233-9558

Preliminary Studies on Double-Diffusive Natural Convection During Physical Vapor Transport Crystal Growth of Hg_2Br_2 for the Spaceflight Experiments

Sung Ho Ha and Geug Tae Kim†

Department of Advanced Materials and Chemical Engineering, Hannam University, 1646, Yuseong-daero, Yuseong-gu, Daejeon, 34054, Korea

(Received 8 January 2019; Received in revised form 7 February 2019; accepted 7 February 2019)

Abstract – We have conducted a preliminary numerical analysis to understand the effects of double-diffusive convection on the molar flux at the crystal region during the growth of mercurous bromide (Hg_2Br_2) crystals in 1 g and microgravity (μg) conditions. It was found that the total molar fluxes decay first-order exponentially with the aspect ratio (AR, transport length-to-width), $1 \le AR \le 10$. With increasing the aspect ratio of the horizontal enclosure from AR = 1 up to Ar = 10, the convection flow field shifts to the advective-diffusion mode and the flow structures become stable. Therefore, altering the aspect ratio of the enclosure allows one to control the effect of the double diffusive natural convection. Moreover, microgravity environments less than 10^{-2}g make the effect of double-diffusive natural convection much reduced so that the convection mode could be switched over the advective-diffusion mode.

Key words: Double-diffusive convection, Physical vapor transport, Hg_2Br_2

1. Introduction

The subject of natural convection in enclosures has been widely recognized and extensive research has been performed. Most available studies have focused on natural convection with thermal gradients in enclosures, which appears in buildings. Some applications have been extended to nuclear reactor systems, materials processing, natural ventilation in buildings, and solar energy. Recently, research has been extended to the transport in porous media [1,2], and to double-diffusive natural convection [3,4]. However, we shall refer to double-diffusive convection relevant to the study of physical vapor transport (PVT) in the ampoules of vapor crystal growth. In general, PVT is well known as a crystal growth process, which has many advantages over conventional crystal process like a melt-growth because it can be performed at low temperatures and provides relatively high interfacial morphological stability [5].

Duval and coworkers [6-18] have computationally attempted to understand the influence of convective parameters on natural convective flow in vapor crystal growth enclosures, e.g., physical vapor transport (PVT) system. They reported that unsteady flow is shown to be correlated with a degradation of crystal quality as quantified by light scattering pattern measurements. An unsteady flow becomes steady (diffusive-advection) in a microgravity environment of 10^{-3} g as predicted by the diffusion-limited model. Duval [12] addressed that there are four regions which distinct flow field structure occur. During the transition from one region to another, three distinct bifurcation events occur. The flow field structure transits from a unidirectional advective-diffusion flow to two cells, subsequently to four cells, and finally six cells. Singh et al. [19, 20] have characterized mercurous bromide crystals grown by the physical vapor transport (PVT) method in closed ampoules within two-zone and multizone crystal growth furnaces. They have reported the materials exhibit an exciting material for acousto-optic tunable filters (AOTF) and Bragg cells suitable for optical signal processing. Mercurous bromide crystals showed a strong cleavage plane in the <110> orientation, and its velocity of the acoustic wave was observed to be 273 m/s. More recently, Amarasinghe et al. [21] grew single crystals of mercurous halides by the physical vapor transport (PVT) method and characterized the orientation and the crystalline quality of the grown crystals using high resolution x-ray diffraction technique. The grown mercurous iodide (Hg_2I_2) crystals are 48 mm in diameter, 400-600 grams in weight and 70-80 mm in height. Mercurous halides are proved to be promising materials in applications for acousto-optic tunable filters (AOTF's) for 8~12 μm wavelength region.

With regard to the physical vapor transport method, Shi et al. [22] prepared 6H-type silicon carbide whiskers and studied both the growth of SiC whiskers and the mechanism of SiC nucleation, and found that there exist two major factors: the sublimation of raw materials, and the transport of the vapor species. Fanton et al. [23] published the results that the addition of hydrogen related to the SiC crystals grown by the PVT techniques had nothing with the level of boron contamination in all samples. Paorici et al. [24] carried out experiments of PVT techniques for urotropine to prove one-dimensional diffusion model to get qualitative results.

In so far as crystal quality is affected by the convection field, it is

† To whom correspondence should be addressed.
E-mail: geugtaekim@gmail.com

important to understand double-diffusive convective flow structure in the vapor phase. In particular, much study of double-diffusive convection is needed as a basis on the ground for future space-flight experiments in South Korea. This motivation causes us to investigate effects of double-diffusive natural convection on PVT for a mixture of Hg_2Br_2 and argon on earth and under microgravity environments. A mixture of Hg_2Br_2 and argon is chosen as a systematic model study for further study into microgravity environments. In this study we investigate computationally the characteristics of the double-diffusive convective flow structures in the PVT processes of Hg_2Br_2 crystal growth.

2. System and Mathematical Formulation

We consider a steady state double diffusive natural convection in PVT crystal growth enclosure caused by the driving force of the vapor crystal growth, e.g., ΔT, the source and the crystal regions, T_s-T_c along with conducting linear temperature profile at wall boundary conditions, as shown schematically in Fig. 1. The mass fluxes of sublimation-condensation at the interfaces, i.e., the finite normal velocities at the interfaces, are expressed by Stefan flow deduced from the one-dimensional diffusion-limited model [25]. The gravitational force vector is aligned in the negative y-direction. The thermophysical properties of the fluid in the vapor phase are assumed to be constant. With regard to the density dependency of the buoyancy term in the momentum equation, the density is calculated through the ideal gas equation of state and is dependent on temperature and pressure. The u_x and u_y denote the velocity components along the x- and y-coordinates in the Cartesian coordinate system (x, y), and T, ω_A, p denote the temperature, mass fraction of species A (Hg_2Br_2) and pressure, respectively, where the superscript of * denotes the dimensionless variable [11,12,13].

The dimensionless variables are scaled as follows:

$$x^* = \frac{x}{H},\quad y^* = \frac{y}{H}, \tag{1}$$

$$u = \frac{u_x}{U_c}, v = \frac{u_y}{U_c}, p = \frac{p}{\rho_c U_c^2}, \tag{2}$$

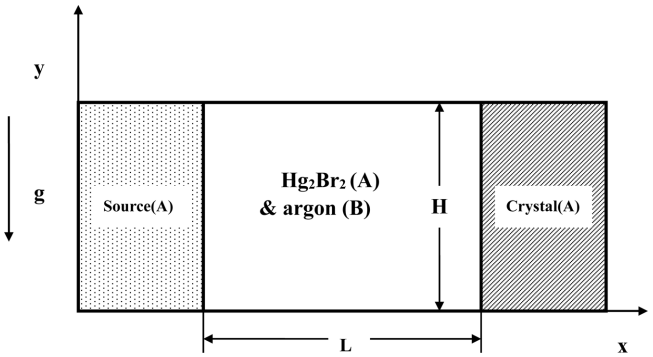

Fig. 1. Schematic and coordinates for modeling and simulation of PVT crystal growth reactor of Hg_2Br_2(A) and argon (B).

$$T^* = \frac{T - T_c}{T_s - T_c}, \omega_A^* = \frac{\omega_A - \omega_{A,c}}{\omega_{A,s} - \omega_{A,c}}. \tag{3}$$

The non-dimensional governing equations in the Cartesian coordinate system (x, y) are given by:

$$\nabla^* \bullet V = 0, \tag{4}$$

$$\vec{V} \bullet \nabla^* \vec{V} = -\nabla^* p^* + Pr \nabla^{*2} \vec{V} - \frac{Gr \cdot Pr^2}{AR^3} \cdot \frac{(1-\rho^*)}{\beta \Delta T}, \tag{5}$$

$$\vec{V} \bullet \nabla^* T^* = \nabla^{*2} T^*, \tag{6}$$

$$\vec{V} \bullet \nabla^* \omega_A^* = \frac{1}{Le} \nabla^{*2} \omega_A^*. \tag{7}$$

The non-dimensional boundary conditions are
On the walls ($0 < x^* < L/H$, $y^* = 0$ and 1):

$$u(x^*, 0) = u(x^*, 1) = v(x^* 0) = v(x^*, 1) = 0$$

$$\frac{\partial \omega_A^*(x^*, 0)}{\partial y^*} = \frac{\partial \omega_A^*(x^*, 1)}{\partial y^*} = 0,$$

$$T^*(x^*, 0) = -\frac{1}{AR} \cdot x^* + 1 \tag{8}$$

On the source ($x^* = 0$, $0 < y^* < 1$):

$$u(0, y^*) = -\frac{1}{Le} \frac{1}{(Cv - 1)} \frac{\partial \omega_A^*(0, y^*)}{\partial y^*},$$

$$v(0, y^*) = 0,$$

$$T^*(0, y^*) = 1,$$

$$\omega_A^*(0, y^*) = 1. \tag{9}$$

On the crystal ($x^* = L/H$, $0 < y^* < 1$):

$$u(L/H, y^*) = -\frac{1}{Le} \frac{1}{(Cv)} \frac{\partial \omega_A^*(L/H, y^*)}{\partial x^*}$$

$$v(L/H, y^*) = 0,$$

$$T^*(L/H, y^*) = 0,$$

$$\omega_A^*(L/H, y^*) = 0. \tag{10}$$

where

$$\text{aspect ratio, } AR = L/H \tag{11a}$$

$$\text{concentration number, } C_v = (1 - \omega_{A,c})/\Delta\omega \tag{11b}$$

$$\text{Lewis number, } Le = \kappa/D_{AB} \tag{11c}$$

$$\text{Prandtl number, } Pr = \nu/\kappa \tag{11d}$$

$$\text{thermal Grashof number, } Gr = g\beta\Delta T H^3/\nu^2 \tag{11e}$$

The Peclet number, Pe is defined as

$$Pe = \frac{U_{adv} L}{D_{AB}}, \tag{11f}$$

which represents the ratio of advective to diffusive flux. The U_{adv} is the streaming velocity based on the sublimation and condensation advective-diffusive flux. When the advective-diffusive flux is dominant, the flow field is stabilized [10]. Pe may be rewritten from

one-dimensional model in the form [26],

$$Pe = \ln\frac{\omega_B(L)}{\omega_B(0)} = \ln\frac{p_B(L)}{p_B(0)}. \quad (11g)$$

In the dimensionless parameters, which appear in the governing equations, the physicochemical properties of the gas mixture are obtained from a gas kinetic theory using Chapman-Enskog's formulas [27], due to lack of available data: the viscosity of and thermal conductivity of argon, the mixture's viscosity and thermal conductivity, the mass diffusivity for binary mixtures. The collision integral functions for estimations of viscosities of Hg_2Br and argon, diffusivity for binary mixture of Hg_2Br and argon can be found in reference [28]. The method of Wilke is used for estimation of the viscosity of Hg_2Br and argon [28]. Because the total vapor pressure is assumed to be constant during the physical vapor transport of Hg_2Br in the vapor phase, the mass fraction of species A (Hg_2Br) is defined as

$$\omega_A = \frac{1}{1+(P_T/p_A-1)M_B/M_A}. \quad (12)$$

The vapor pressure [29] p_A of Hg_2Br_2 (in the unit of Pascal) can be evaluated from the following formula as a function of temperature:

$$p_A = e^{(a-b/T)}, \quad (13)$$

in which a = 9.956, b = 4563. P_T denotes the total pressure, and the partial pressures for A(B) are denoted by p_A (p_B). Invoking of the Boussinesq approximation of the density [11] yields.

$$\rho = \overline{\rho}(1-\beta\Delta T+\tau\Delta\omega),$$

where β is the coefficient of thermal volume expansion, and γ is the coefficient of solutal volume expansion,

$$\beta = -\frac{1}{\rho}\left(\frac{\partial\rho}{\partial T}\right)_{\omega_A}, \quad \tau = \frac{1}{\rho}\left(\frac{\partial\rho}{\partial\omega}\right)_T.$$

The ratio of thermal and solutal buoyancy forces [30] is defined as

$$N = \frac{-\tau\Delta\omega}{\beta\Delta T}. \quad (14)$$

To solve the discretization equations for the system of nonlinear, coupled governing partial differential equations, the semi-implicit method pressure-linked equations revised (SIMPLER) algorithm proposed by Patankar [31] with a power law scheme was used. A 43 × 23 ($x \times y$) and a 63 43 × 23 ($x \times y$) grid system were used for AR = 1 and AR ≥ 2, respectively. The iteration procedure was continued until the following convergence criterion was satisfied:

$$\left|\frac{\phi_{j+1}-\phi_j}{\phi_j}\right| < 10^{-5}, \text{ for all } \phi,$$

where ϕ represents any dimensionless dependent variable being computed, e.g., u,v,T^* and ω_A^*, and j refers to the value of ϕ at the jth iteration level. The numerical verifications of our results have been done in references [13,16,17].

3. Results and Discussion

For the system at hand, we are interested in double-diffusive convection physical vapor transport with the presence of impurity, argon. When the $M_A \neq M_B$ is modeled, i.e., the molecular weight of component A is not equal to that of component B, the solutal convection is important, in particular when the imposed temperature profile has little effect on the total molar flux. The double-diffuisve convection flow structure can be quantified by the seven dimensionless governing parameters of aspect ratio (AR, L/H), concentration number (Cv, $(1-\omega_{A,c})/\Delta\omega$), Lewis number (Le, κ/D_{AB}), Peclet number (Pe, $U_{adv}L/D_{AB}$), Prandtl number (Pr, n/k), thermal Grashof number (Gr$_t$, $g\beta\Delta TH^3/\nu^2$), and solutal Grashof number (Gr$_s$, $g\gamma\Delta\omega H^3/\nu^2$) [11].

The excess pressure of the impurity component affects the binary diffusion coefficient, which determines the advective-diffusion flux at the interfaces. However, we restrict our study to investigating how a double-diffusive convection flow will affect the molar flux and its distribution across an interface in the crystal region. Thus, the effects of the parameters of excess pressure of the impurity, argon and the molecular weight, total pressure on the double diffusion natural convection are not examined in this study. Throughout the computational works in this study, the source temperature, T_s = 290 °C and width H = 2 cm are fixed, and the characteristic length H is introduced in the calculations of thermal and solutal Grashof numbers. Numerical results are presented in the form of velocity vectors, streamlines, and iso-mass fraction contours, and

Fig. 2 shows the effects of aspect ratio, AR (L/H) on the total molar flux of Hg_2Br_2 in terms of moles $cm^{-2}s^{-1}$ for various aspect ratio, 1 ≤ AR ≤ 10, based on ΔT = 30 °C (290 °C→260 °C), and 1 g,

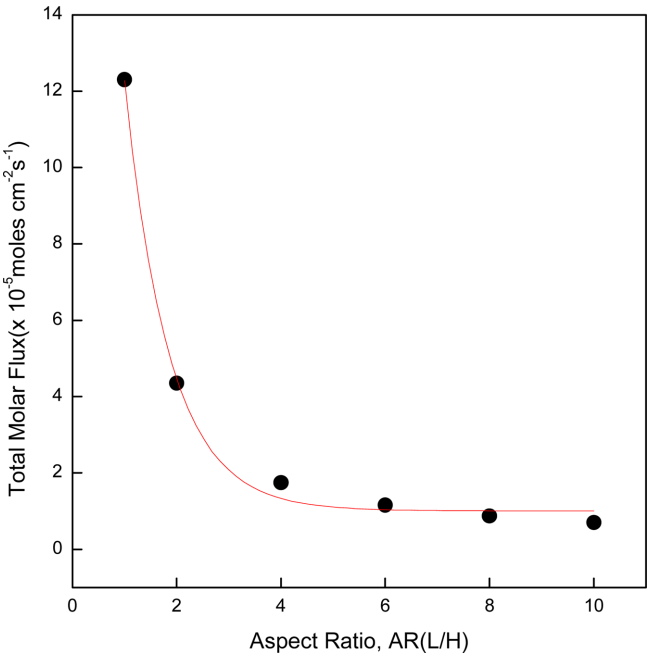

Fig. 2. Effects of aspect ratio (AR, L/H) on the total molar flux (moles $cm^{-2}s^{-1}$) of Hg_2Br_2, based on ΔT = 30 °C (290 °C→260 °C), 1 g, P_B = 10 Torr, Pr = 0.99, Le = 0.23, C_v = 1.07, Pe = 2.64, Gr$_t$ = 2.8 × 10^3, Gr$_s$ = 4.4 × 10^4.

one gravity acceleration (where 1 g = 980.665 cm s^{-2}), P_B = 10 Torr, Pr = 0.99, Le = 0.15, C_v = 1.31, Pe = 1.4, $Gr_t = 2.26 \times 10^3$, $Gr_s = 3.87 \times 10^4$. Note that the governing dimensionless parameters of Prandtl, Lewis, concentration, Peclet, and Grashof numbers are obtained for the mixture of Hg_2Br_2 and argon, in Fig. 2 through Fig. 11. As plotted in Fig. 2, the total molar fluxes decay first-order exponentially with the aspect ratio, $1 \le AR \le 10$. For the range of $1 \le AR \le 2$, the molar fluxes drop significantly, and, for $2 \le AR \le 10$, decrease slowly. So, the total molar fluxes decrease very sharply near AR = 1, and, then since AR = 2, decrease. With increasing the aspect ratio, the wall effects result in a decrease in the molar flux, which is consistent with the previous results [12,32]. It is found that the total mass flux occurs at the square cavity, and as we approach the horizontal narrow cavity AR = 10, the total mass flux decreases, which is reflected in the double diffusion convective flow fields, as addressed later, in Figs. 3 through 5. Therefore, the double-diffusive convection can be operated by altering the aspect ratio of the growth ampoule.

Figs. 3 through 5 show that (a) velocity vector, (b) streamline, (c) temperature, and (d) mass fraction profile for three cases of AR = 1, 2, and 8, ΔT = 30 °C (290 °C→260 °C), and 1 g. As depicted in Figs. 3 and 4, the single double diffusive convection unicellular flow structure occurs in the vapor phase and the convection flows toward the crystal interface in the lower half of the enclosure, which results in providing this part of the crystal interface with vapor supersaturated in component of Hg_2Br_2. The counter-clockwise single cell indicates the major role of the double-diffusive convection, because thermal convection alone, with the left part of the enclosure warmer than the right part, would result in an oppositely rotating cell, and thus, in augmented total molar flux in the upper half of the crystal interface [33]. The unicellular convective flow is asymmetrical along both the x-direction and the y-direction, which shows the dominating convection flow field. The flow field looks like the advective-diffusion mode along the bottom side wall because of the side wall effects damping the convection. Figs. 3(c) and 4(c) illustrate changes in which isotherms are positioned in the main part of the enclosure and convection near the crystal interface is transited into conduction. Moreover, it is observed from iso-mass fractions in 3(d) and 4(d) that the diffusion-limited mechanism is a critical factor in the crystal growth in the crystal interface because the intervals between iso-mass fractions near the crystal interface is tightly narrow so that the

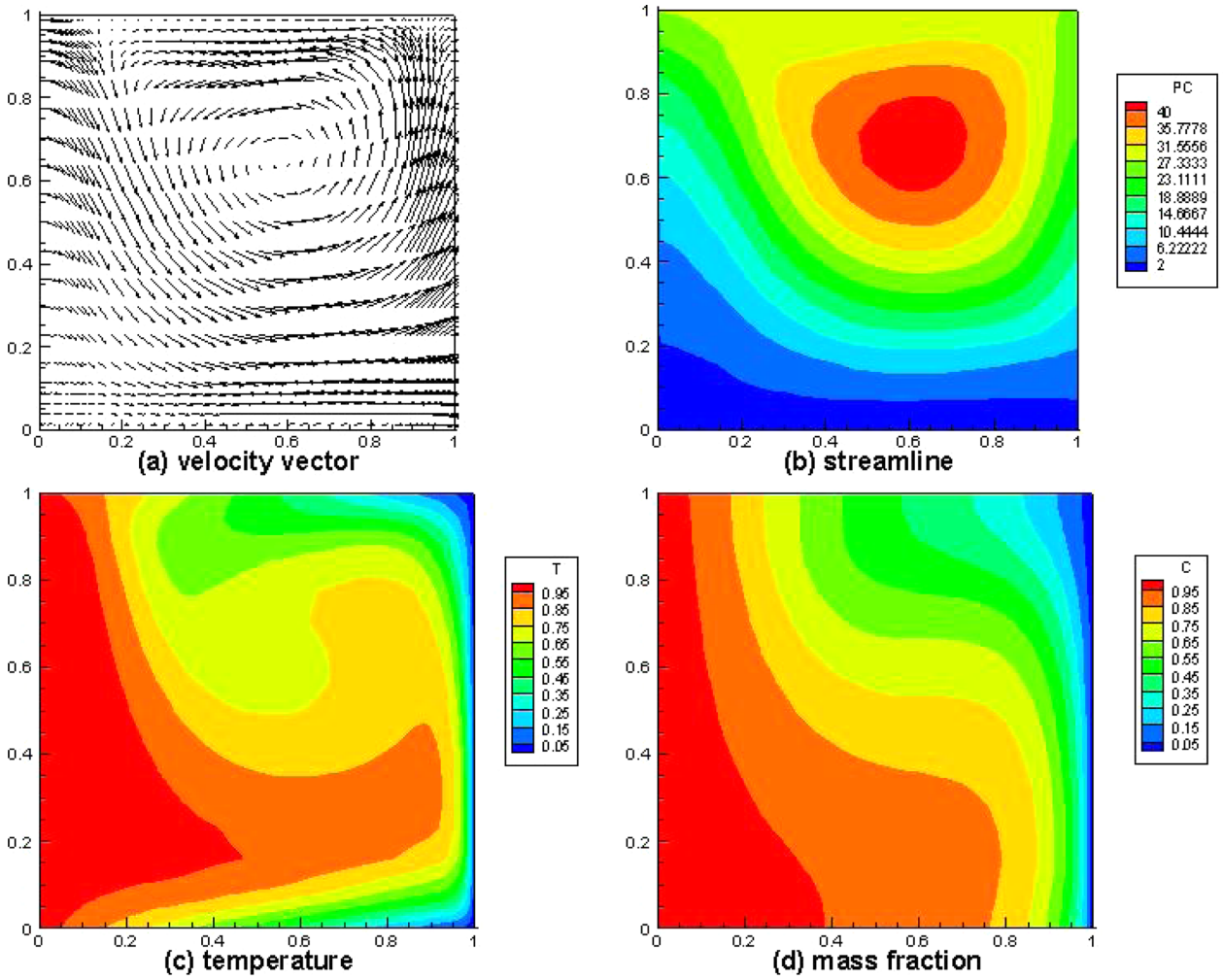

Fig. 3. (a) velocity vector profile, (b) streamline profile, (c) temperature profile, (d) mass fraction profile, based on ΔT = 30 °C (290 °C→260 °C), 1 g, P_B = 10 Torr, Pr = 0.99, Le = 0.23, C_v = 1.07, Pe = 2.64, $Gr_t = 2.8 \times 10^3$, $Gr_s = 4.4 \times 10^4$. The dimensional maximum magnitude of velocity vector is 18.03 cm s^{-1}.

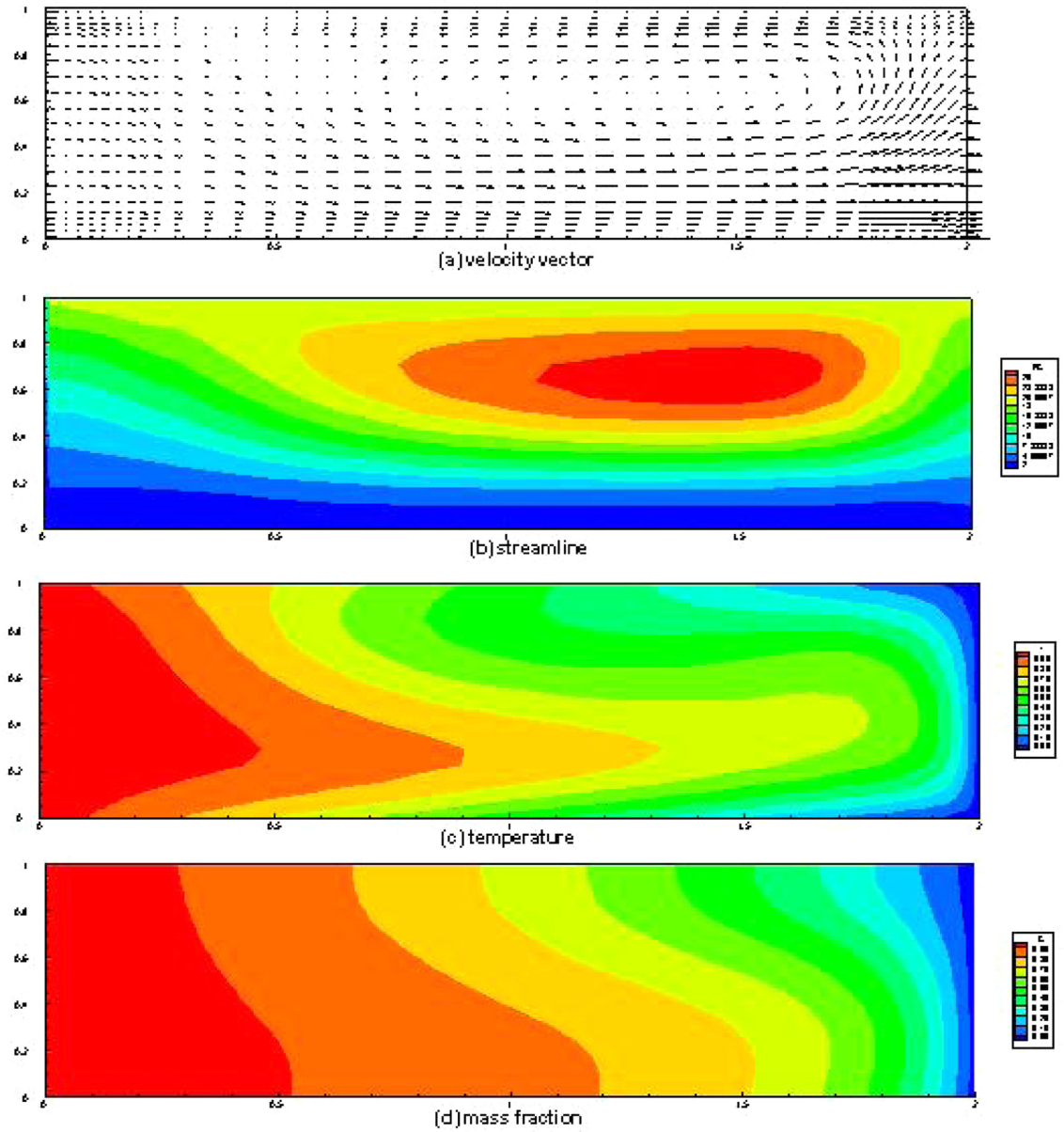

Fig. 4. (a) velocity vector profile, (b) streamline profile, (c) temperature profile, (d) mass fraction profile, based on ΔT = 30 °C (290 °C→260 °C), 1 g, P_B = 10 Torr, Pr = 0.99, Le = 0.23, C_v = 1.07, Pe = 2.64, $Gr_t = 2.8 \times 10^3$, $Gr_s = 4.4 \times 10^4$. The dimensional maximum magnitude of velocity vector is 5.28 cm s^{-1}.

convection is switched over diffusion.

With increasing the aspect ratio of the horizontal enclosure from AR = 1 and 2 to AR = 8, as illustrated in Figs. 3 through 5, the convection field transits from the convection to the advective-diffusion mode and, the velocity and streamline fields become stable and exhibit the advective-dffusion dominated flow. It is due to fact that the wall effects enhance the viscous force which would alleviate the effects of the convection. The velocity vector, Fig. 5(a) and streamline profile, Fig. 5(b), show the parabolic advective-diffusion profile. The isotherms in Fig. 5(c) and the iso-mass fraction in Fig. 5(d) are well equally placed, supporting the advective-diffusion model.

Fig. 6 shows the relationship between total molar flux (moles $cm^{-2}s^{-1}$) of Hg_2Br_2 and the temperature difference between the source and the crystal regions, 10 °C ≤ ΔT ≤ 50 °C, based on AR = 1, T_s = 290 °C fixed, 1 g, P_B = 10 Torr, $1.8 \times 10^3 \le Gr_t \le 2.9 \times 10^3$, $2.6 \times 10^4 \le Gr_s \le 4.9 \times 10^4$. As shown in Fig. 6, the total molar flux of Hg_2Br_2 for 10 °C ≤ ΔT ≤ 50 °C, has a direct and linearly relationship with the temperature difference, ΔT. For 10 °C ≤ ΔT ≤ 30 °C, the total molar flux is significantly dependent on the temperature difference, while for 30 °C ≤ ΔT ≤ 50 °C, it varies slightly with the temperature difference. The temperature gradient for 10 °C ≤ ΔT ≤ 30 °C is, 8.5×10^{-6} moles $cm^{-2}s^{-1}K^{-1}$ and for 10 °C ≤ ΔT ≤ 50 °C, 1.7×10^{-6} moles $cm^{-2}s^{-1}K^{-1}$. Therefore, the temperature gradient for 10 °C ≤ ΔT ≤ 30 °C is greater than for 30 °C ≤ ΔT ≤ 50 °C by a factor of 5. With increasing the driving force of PVT crystal growth, i.e., DT, the temperature difference between the source and the crystal, an increase of total molar

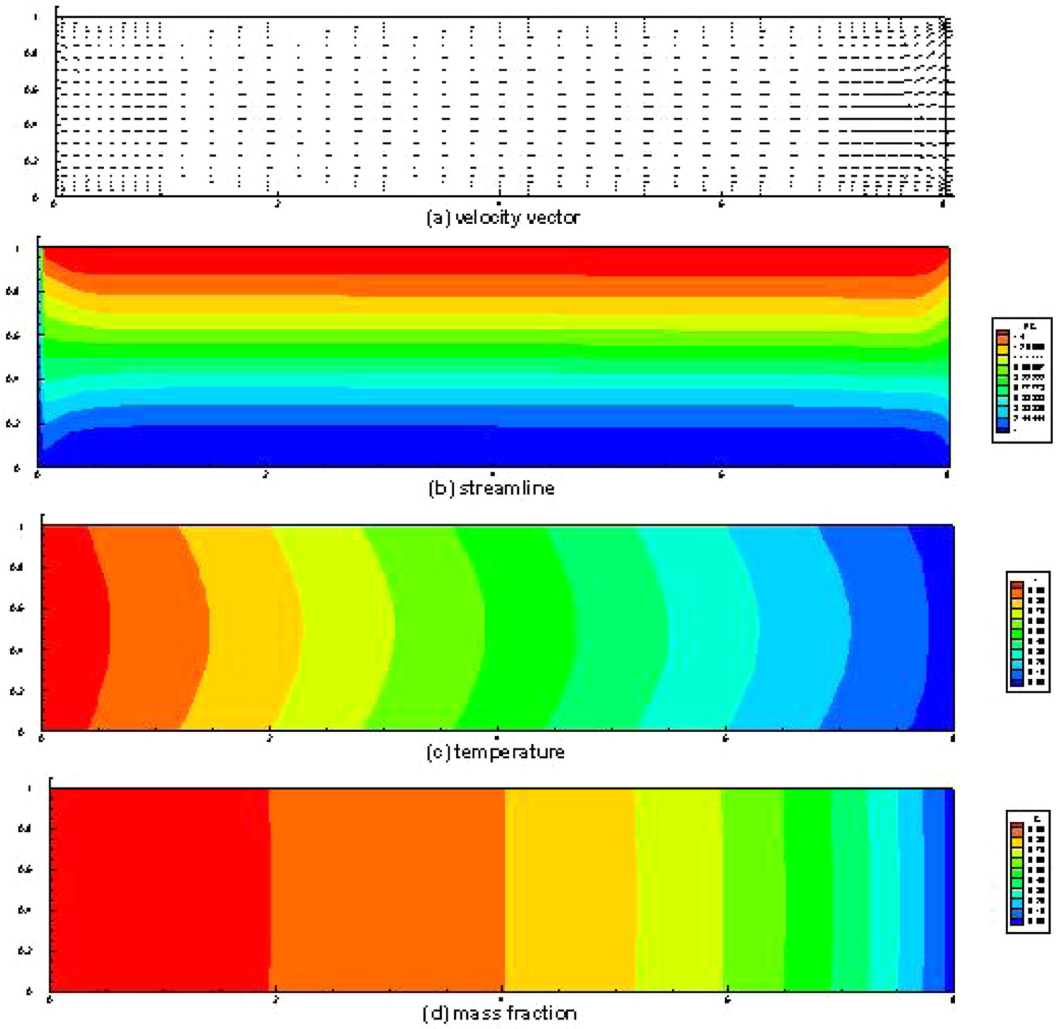

Fig. 5. (a) velocity vector profile, (b) streamline profile, (c) temperature profile, (d) mass fraction profile, based on $\Delta T = 30\ ^{o}C$ (290 $^{o}C \rightarrow 260\ ^{o}C$), 1 g, $P_B = 10$ Torr, Pr = 0.99, Le = 0.23, $C_v = 1.07$, Pe = 2.64, $Gr_t = 2.8 \times 10^3$, $Gr_s = 4.4 \times 10^4$. The dimensional maximum magnitude of velocity vector is 0.63 cm s^{-1}.

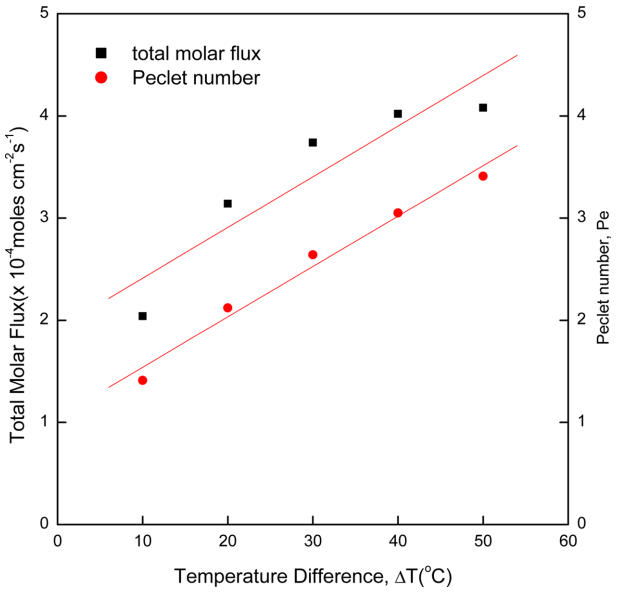

Fig. 6. Relationship of total molar flux of Hg_2Br_2 in terms of moles $cm^{-2}s^{-1}$ and the temperature difference, ΔT (^{o}C), Peclet number, Pe, based on AR = 1, $T_s = 290\ ^{o}C$ fixed, 1 g, $P_B = 10$ Torr, $1.8 \times 10^3 \le Gr_t \le 2.9 \times 10^3$, $2.6 \times 10^4 \le Gr_s \le 4.9 \times 10^4$.

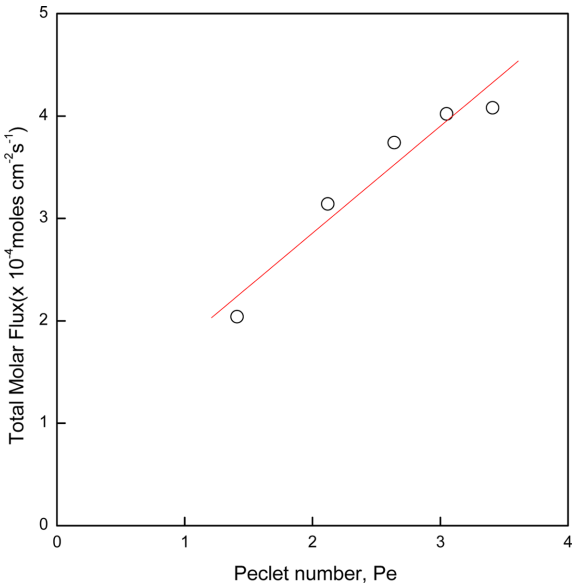

Fig. 7. Total molar flux of Hg_2Br_2 as a function of the dimensionless Peclet number, Pe, corresponding to Fig. 6, based on AR = 1, $T_s = 290\ ^{o}C$ fixed, 1 g, $P_B = 10$ Torr, $1.8 \times 10^3 \le Gr_t \le 2.9 \times 10^3$, $2.6 \times 10^4 \le Gr_s \le 4.9 \times 10^4$.

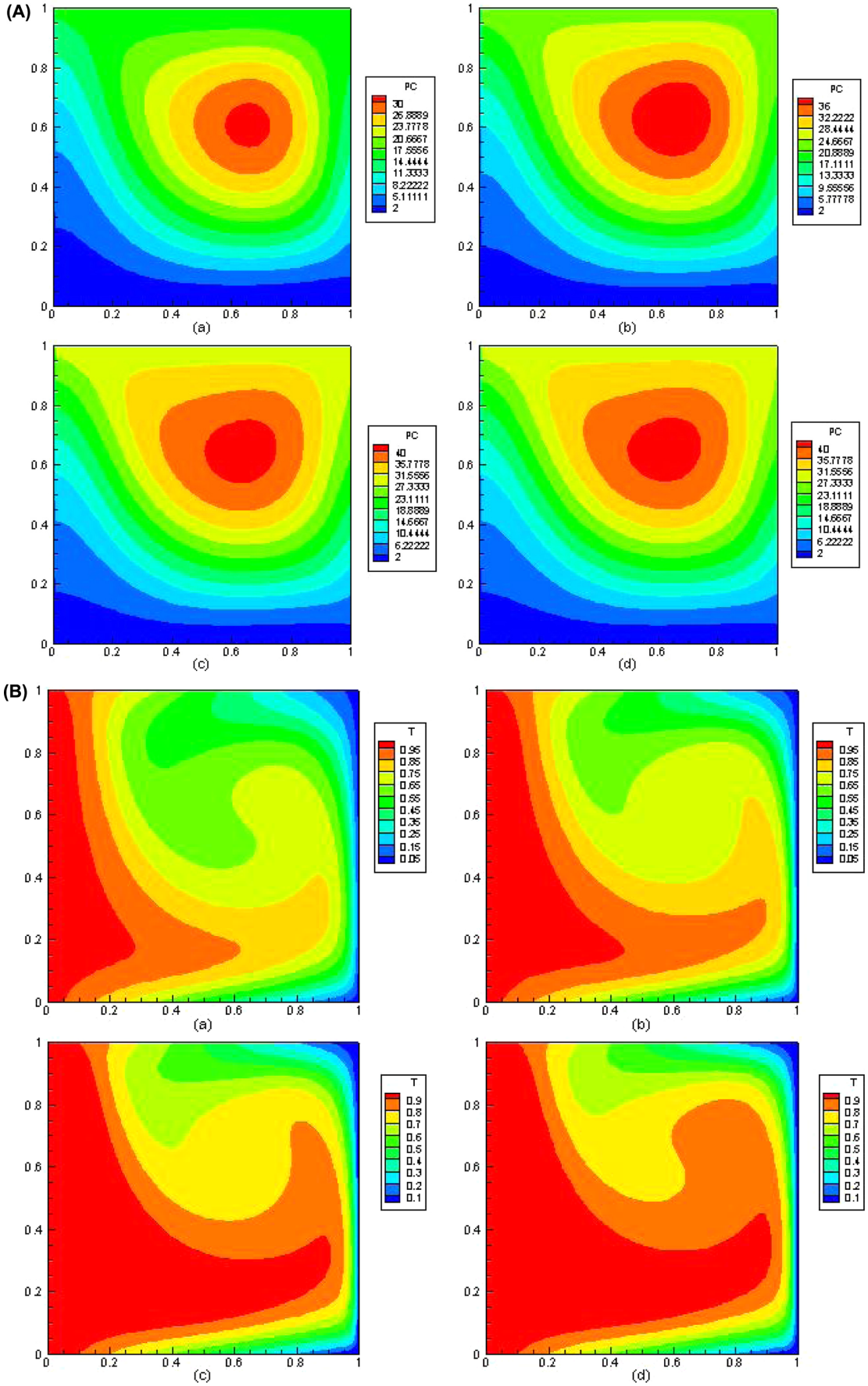

Fig. 8. (A) Streamline profile: (a) ΔT = 10 °C, (b) ΔT = 20 °C, (c) ΔT = 40 °C, (d) ΔT = 50 °C, based on AR = 1, 1 g and PB = 10 Torr. (B) Temperature profile: (a) ΔT = 10 °C, (b) ΔT = 20 °C, (c) ΔT = 40 °C, (d) ΔT = 50 °C, based on AR = 1, 1 g and PB = 10 Torr.

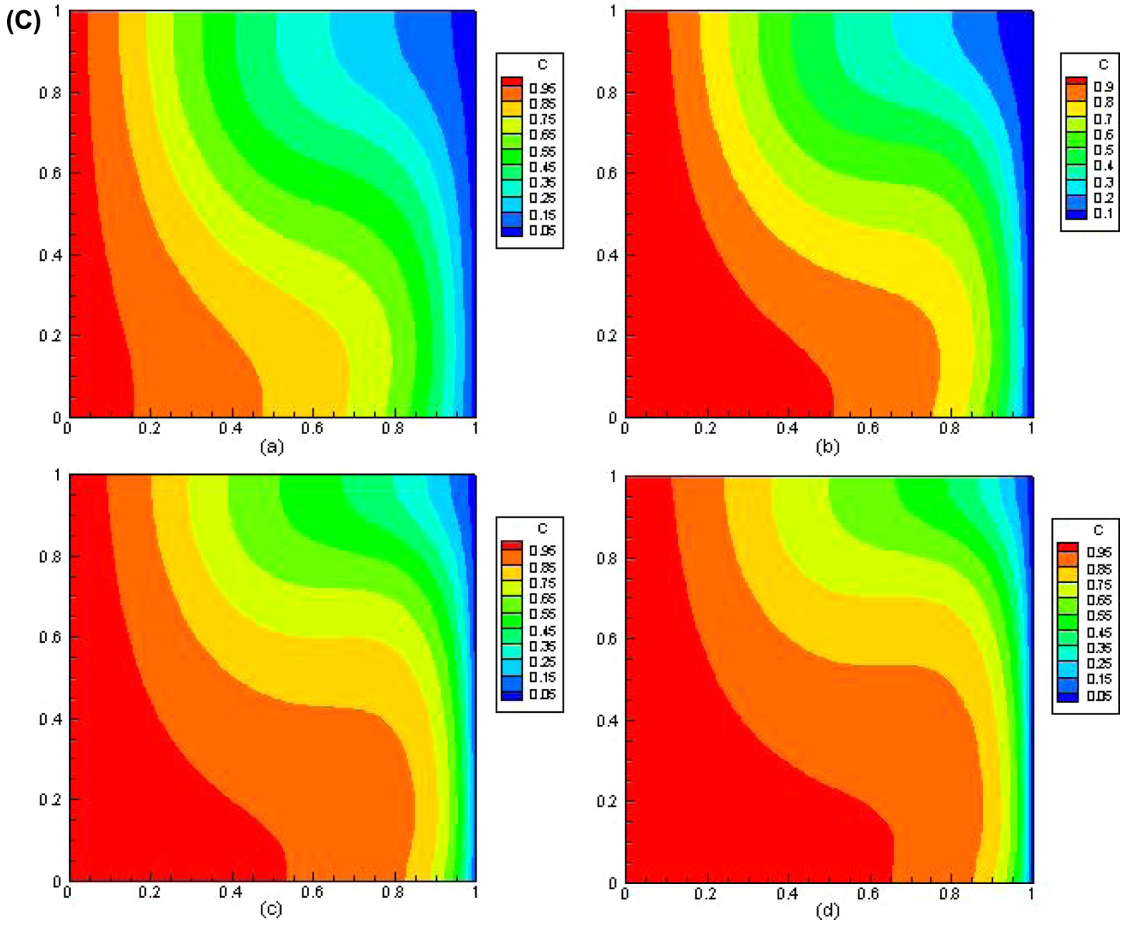

Fig. 8. (continued) (C) Mass fraction profile: (a) ΔT = 10 °C, (b) ΔT = 20 °C, (c) ΔT = 40 °C, (d) ΔT = 50 °C, based on AR = 1, 1 g and PB = 10 Torr.

fluxes is strongly reflected for the low temperature differences, 10 °C ≤ ΔT ≤ 30 °C, because of thermally buoyancy-driven convection. On the other hand, the effects of thermally buoyancy-driven convection are weakened for 30 °C ≤ ΔT ≤ 50 °C. As observed clearly in Figs. 8(a), 8(b), and 8(c), there are little changes in streamlines and isotherms and iso-mass fractions. In Fig. 6, the relation between the temperature difference and Peclet number is found to be direct and linear. Note that the Peclet number is related to thermodynamic variables [26].

Fig. 7 shows the relationship between total molar flux (moles $cm^{-2}s^{-1}$) of Hg_2Br_2 and the Peclet number, corresponding to Fig.6. Also, there is a direct and linear relationship between the total molar flux of Hg_2Br_2 and the Peclet number. Peclet number is used instead of the thermal Grashof number, because with increasing the temperature difference between the source and the crystal, at the source temperature of 290 °C fixed, the inverse value of the square corresponding kinematic viscosity, $1/\nu^2$ increases so that the thermal Grashof number is not considered as a quantity parameter in this study. The study of thermal properties on thermal convection would remain for further research in the future. The gradient of total mass flux to Peclet number is 1.02 moles $cm^{-2}s^{-1}$. Also, for considering the buoyancy parameter which is defined in Equation (14), N = -17 at ΔT = 10 °C, and the opposing buoyancy-induced boundary flows are expected.

Figs. 8(a), 8(b) and 8(c) show iso-streamlines, and isotherms, and iso-mass fractions, for four different temperature differences, AR = 1, 1 g, and PB = 10 Torr. As shown in Fig. 8(a), there occurs a single unicellular convective roll for the process conditions, and the convective roll exhibits asymmetrical against the center lines of $x^* = 0.5$, and $y^* = 0.5$, and the cell is in counter-clockwise, refer to Fig. 3(a). As mentioned, there is little variation in the structure and streamline value, temperature, and mass fraction for two cases of (c) ΔT = 40 °C and (d) ΔT = 50 °C, through the Figs. 8(a) through (c).

Fig. 9 shows the total molar flux of Hg_2Br_2 in terms of moles cm^{-2} s^{-1} as a function of gravity acceleration, 10^{-5} g ≤ g_y ≤ 1 g, based on AR = 1, ΔT = 50 °C (290 °C→240 °C), and PB = 10. The double diffusive convection is dominated over the advection-diffusion for 10^{-2} g ≤ g_y ≤ 1 g. The convection mode shifts into diffusion down to $g_y = 10^{-2}$ g and, from $g_y = 10^{-2}$ g, down to $g_y = 10^{-5}$ g, the diffusion becomes predominant. As seen in Fig. 9, the total molar fluxes drop sharply for 10^{-2} g ≤ g_y ≤ 1 g. This indicates the mass transport is diffusion-dominated under the microgravity environments less than 10^{-2} g. This tendency is approximately consistent with previous results [34,35]. Duval et al. [15] presented that an unsteady flow becomes diffusive-advective flow under microgravity environments of gravity levels less than 10^{-3} g, and Nadarajah et al. [33] suggested 10^{-1} g an adequate level for diffusive transport. We can see that the effect of double dif-

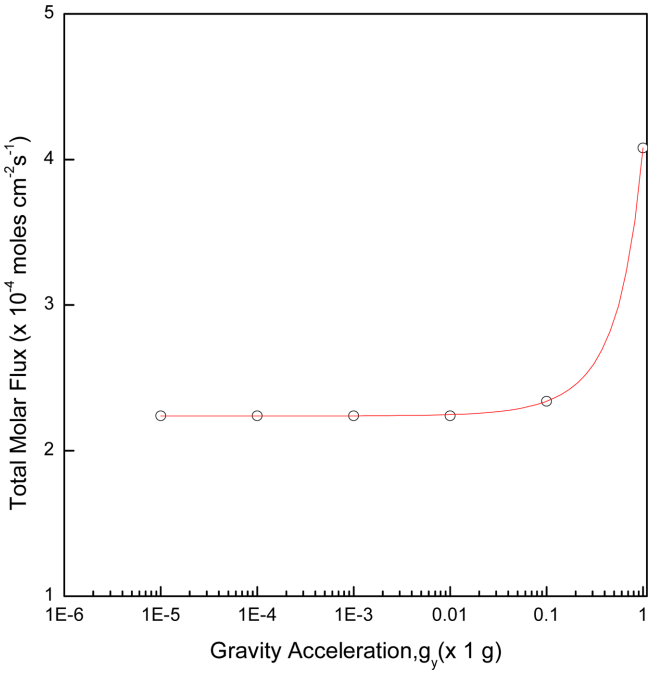

Fig. 9. Total molar flux of Hg_2Br_2 in terms of moles $cm^{-2}s^{-1}$ as a function of gravity acceleration, 10^{-5} g ≤ g_y ≤ 1 g, based on AR = 1, ΔT = 50 °C (290 °C→240 °C), and P_B = 10, Pr = 0.97, Le = 0.37, C_v = 1.03, Pe = 3.41.

fusive convection is first important and then decreases rapidly and eventually the mode of transport becomes purely diffusion. Since the gravitational parameter is very important, a thorough understanding of double diffusive convection would be required for future spaceflight experiments in South Korea. Fig. 10 shows (a) velocity vector profile, (b) streamline profile, (c) temperature profile, (d) mass fraction profile, based on AR = 1, ΔT = 50 °C (290 °C→240 °C), 10^{-3} g and PB = 10. The dimensional maximum magnitude of velocity vector of 7.63 cm s^{-1} is obtained. The velocity vector and streamline profiles in Figs. 10(a) and (b) exhibit a typical advective-diffusion pattern. Energy is transported through conduction near the crystal interface because the tight fine intervals of isotherms appear in the neighborhood of the crystal region, while the vapor of Hg_2Br_2 is transported through the diffusion mechanism in the neighborhood of the crystal interface due to the tight fine intervals of iso-mass fractions. Not shown here, there are little changes in streamlines, isotherms and iso-mass fraction contours for 10^{-2} g and 10^{-3} g cases.

To examine the effect of gravity accelerations on the interfacial distributions of total molar flux (moles $cm^{-2}s^{-1}$) of Hg_2Br_2, interfacial distributions of molar flux (moles $cm^{-2}s^{-1}$) of Hg_2Br_2 for four gravity accelerations (1 g, 10^{-1} g, 10^{-2} g, and 10^{-3} g, where 1 g = 980.665 cm s^{-2}), based on AR = 1, ΔT = 50 °C (290 °C→240 °C), and PB = 10 are pre-

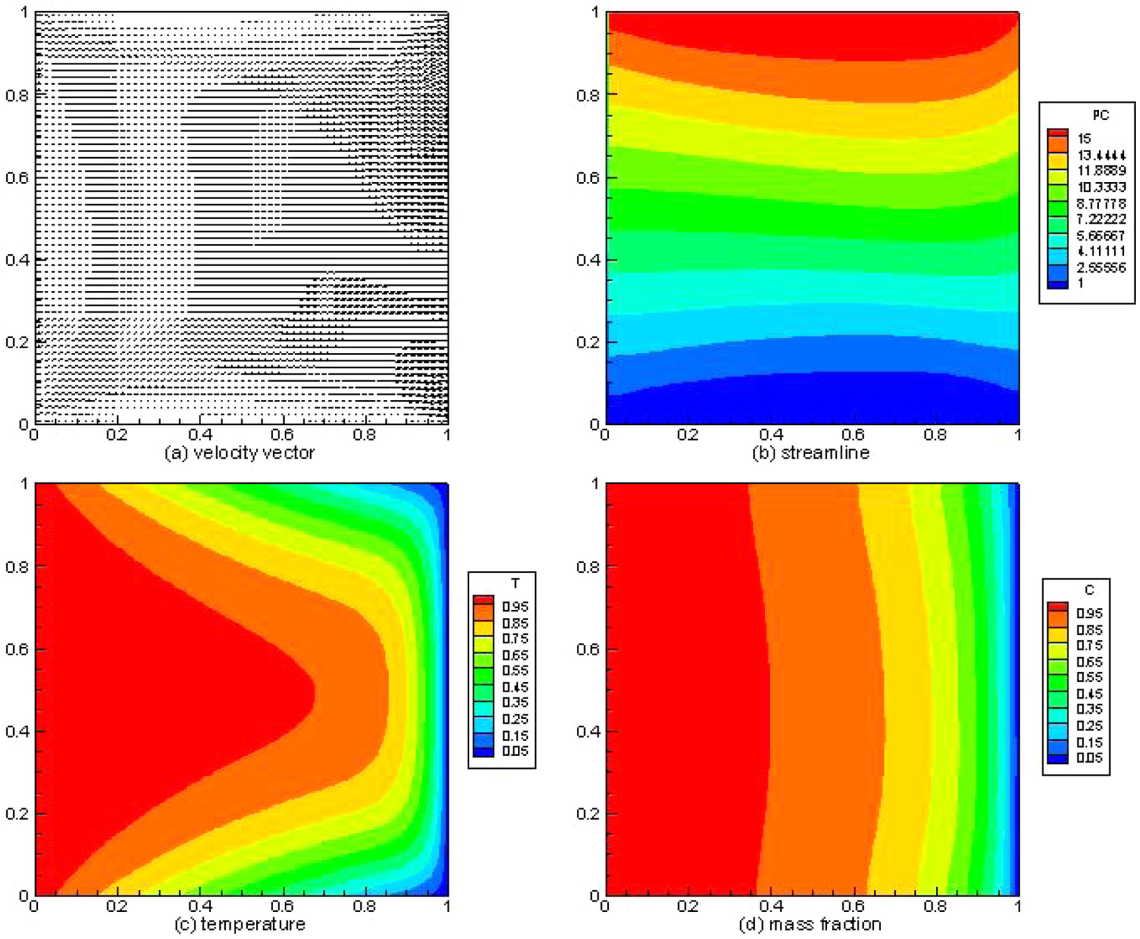

Fig. 10. (a) velocity vector profile, (b) streamline profile, (c) temperature profile, (d) mass fraction profile, based on AR = 1, ΔT = 50 °C (290 °C→240 °C), 10^{-3} g, P_B = 10, Pr = 0.97, Le = 0.37, C_v = 1.03, Pe = 3.41. The dimensional maximum magnitude of velocity vector is 7.63 cm s^{-1}.

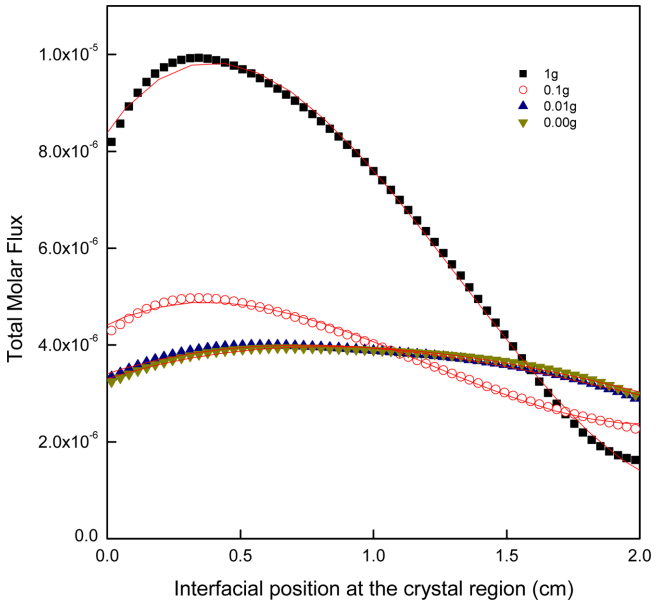

Fig. 11. Interfacial distributions of total molar flux (moles $cm^{-2}s^{-1}$) of Hg_2Br_2 for four gravity accelerations (1 g, 10^{-1} g, 10^{-2} g, and 10^{-3} g, where 1 g = 980.665 cm s^{-2}), based on AR = 1, ΔT = 50 °C (290 °C→240 °C), P_B = 10, Pr = 0.97, Le = 0.37, C_v = 1.03, Pe = 3.41.

sented in Fig. 11. We can see from Fig. 11 that double diffusive convection enhances the overall mass transport of component A, Hg_2Br_2 and consequently also the total mass flux, but at the expense of resulting crystal uniformity in the total mass flux. The effects of double diffusive convection are reflected through the density gradient and binary diffusivity coefficient. The total molar flux along the interfacial position at the crystal for 1 g and 10^{-1} g has asymmetrical profiles at the center position y = 1.0 cm, which indicates three-dimensional convective flow and the presence of single unicellular roll. For 10^{-2} g, and 10^{-3} g, the total mass flux profiles look to be symmetrical at the center position y = 1.0 cm, which implies the advective-diffusion convection in the enclosure is predominant over the double diffusion convection. The convection is found to be directly and intimately related to the non-uniformity of crystal quality desired.

4. Conclusions

It is concluded that the total molar fluxes decay first-order exponentially with the aspect ratio, 1 ≤ AR ≤ 10. With increasing the aspect ratio of the horizontal enclosure from AR = 1 up to AR = 10, the convection field changes from the convection to the advective-diffusion mode and the flow structures become stable. Microgravity environments less than 10^{-2}g make the effect of double-diffusive convection much reduced, so that adequate advective-diffusion transport can be obtained. Double diffusive natural convection flow structures are single unicellular roll and three-dimensional flow pattern. The total molar flux of Hg_2Br_2 for 10 °C ≤ ΔT ≤ 50 °C, has a direct and linear relationship with the temperature difference, ΔT. Boundary flows are expected because of the opposing buoyancy effects (the buoyancy parameter N < 0) for 10 °C ≤ ΔT ≤ 50 °C.

Acknowledgment

This work was financially supported by 2018 Hannam University Research Fund (Project Number: 2018A009).

Nomenclature

A : component A, Hg_2Br_2
B : component B, argon
D_{AB} : diffusivity of A and B
g : standard gravitational acceleration constant, 980.665 cms^{-2}
H : height (cm)
L : transport length, width (cm)
M : molecular weight of component A, B
P : pressure
P_T : total pressure
T : temperature
ΔT : temperature difference between source and crystal, T_s-T_c
Δω : mass fraction difference between source and crystal, $\omega_{A,s}$-$\omega_{A,c}$
x : x-coordinate
y : y-coordinate
u : dimensionless x-component velocity
U_{adv} : characteristic velocity based on the diffusive-advective flux
U_c : characteristic velocity, k/H
$|U|_{max}$: dimensional maximum magnitude of velocity vector
v : dimensionless y-component velocity
u_x : x-component velocity
u_y : y-component velocity
V : velocity vector

Subscripts and Superscripts

A : component A, Hg_2Br_2
Adv : advection
B : component B, Ar
c : crystal
s : source
T : total vapor pressure
* : dimensionless

Greek Letters

β : coefficient of thermal volume expansion
γ : coefficient of solutal volume expansion
κ : thermal diffusivity
ν : kinematic viscosity
∇^* : $(\partial/\partial x^*) + (\partial/\partial y^*)$
∇^{*2} : $(\partial^2/\partial x^{*2}) + (\partial^2/\partial y^{*2})$
ϕ : variable (u, v, T*, ω_A^*)
ω : mass fraction meaning dimensionless mass concentration
ρ : density of fluid with component A and B

References

1. Pippal, S. and Bera, P., "A Thermal Non-Equilibrium Approach for 2D Natural Convection due to Lateral Heat Flux: Square as well as Slender Enclosure," *Int. J. Heat Mass Transf.*, **56**, 501-515(2013).
2. Khadiri, A., Bennacer, R., Hasnaoui, M. and Amahmid, A., "Two- and Three-Dimensional Multiple Steady States in a Porous Cavity Heated and Salted from Below," *Int. J. Therm. Sci.*, **50**, 918-929(2011).
3. Nikbakhti, R. and Rahimi, A. B., "Double-Diffusive Natural Convection in a Rectangular Cavity with Partially Thermally Active Side Walls," *J. Taiwan Inst. Chem. Eng.*, **43**, 535-541(2012).
4. Nithyadevi, N. and Yang, R. J., "Double Diffusive Natural Convection in a Partially Heated Enclosure with Soret and Dufour Effects," *Int. J. Heat Fluid Flow*, **30**, 902-910(2009).
5. Rosenberger, F., "Fluid Dynamics in Crystal Growth from Vapors," *PhysicoChemical Hydrodynamics*, **1**, 3-26(1980).
6. Kassemi, M. and Duval, W. M. B., "Interaction of Surface Radiation with Convection in Crystal Growth by Physical Vapor Transport," *J. Thermophys. Heat Transfer*, **4**, 454-461(1989).
7. Singh, N. B. and Duval, W. M. B., "Growth Kinetics of Physical Vapor Transport Processes: Crystal Growth of the Optoelectronic Material Mercurous Chloride," NASA Technical Memorandum 103788 (1991).
8. Mennetrier, C. and Duval, W. M. B., "Thermal-Solutal Convection with Conduction Effects Inside a Rectangular Enclosure," NASA Technical Memorandum 105371(1991).
9. Mennetrier, C., Duval, W. M. B. and Singh, N. B., "Physical Vapor Transport of Mercurous Chloride Under a Nonlinear Thermal Profile," NASA Technical Memorandum 105920(1992).
10. Duval, W. M. B., "Convective Effects during the Physical Vapor Transport Process-I : Thermal Convection," *J. Mater. Proc. Manufacturing Sci.,* **1**, 83-104(1992).
11. Duval, W. M. B., "Convective Effects during the Physical Vapor Transport Process-II : Thermosolutal Convection," *J. Mater. Proc. Manufacturing Sci.*, **1**, 295-313(1993).
12. Duval, W. M. B., "Transition to Chaos in the Physical Transport Process-I," the Proceeding of the ASME-WAM Winter Annual meeting, Fluid Mechanics Phenomena in Microgravity, ASME-WAM, Nov. 28-Dec. 3, New Orleans, Louisiana(1993).
13. Kim, G. T., Duval, W. M. B., Singh, N. B. and Glickman, M. E., "Thermal Convective Effects on Physical Vapor Transport Growth of Mercurous Chloride Crystals (Hg_2C1_2) for Axisymmetric 2-D Cylindrical Enclosure," *Modelling. Simul. Mater. Sci. Eng.,* **3**, 331-357(1995).
14. Zhou, H., Zebib, A., Trivedi, S. and Duval, W. M. B., "Physical Vapor Transport of Zinc-Telluride by Dissociative Sublimation," *J. Crystal Growth,* **167**, 534-542(1996).
15. Duval, W. M. B., Glicksman, M. E. and Singh, N. B., "Physical Vapor Transport of Mercurous Chloride Crystals; Design of a Microgravity Experiment," *J. Crystal Growth,* **174**, 120-129(1997).
16. Kim, G. T., Duval, W. M. B. and Glicksman, M. E., "Thermal Convection in Physical Vapour Transport of Mercurous Chloride (Hg_2Cl_2) for Rectangular Enclosures," *Modelling. Simul. Mater. Sci. Eng.,* **5**, 289-309(1997).
17. Kim, G. T., Duval, W. M. B. and Glicksman, M. E., "Effects of Asymmetric Temperature Profiles on Thermal Convection during Physical Vapor Transport of Hg_2Cl_2," *Chem. Eng. Comm.,* **162**, 45-61(1997).
18. Tebbe, P. A., Loyalka, S. K. and Duval, W. M. B., "Finite Element Modeling of Asymmetric and Transient Flow Fields during Physical Vapor Transport," *Finite Elements in Analysis and Design,* **40**, 1499-1519(2004).
19. Singh, N. B., Gottlieb, M., Goutzoulis, A. P., Hopkins, R. H. and Mazelsky, R., "Mercurous Bromide Acousto-Optic Devices," *J. Crystal Growth*, **89**, 527-530(1988).
20. Singh, N. B., Marshall, M., Gottlieb, M., Brandt, G. B., Hopkins, R. H., Mazelsky, R., Duval, W. M. B. and Glicksman, M. E., "Purification and Characterization of Mercurous Halides," *J. Crystal Growth*, **106**, 61-67(1990).
21. Amarasinghe, P. M., Kim, J. S., Chen, H., Trivedi, S., Qadri, S. B., Soos, J., Diestler, M., Zhang, D., Gupta, N., Jensen, J. L. and Jensen, J., "Growth of High Quality Mercurous Halide Single Crystals by Physical Vapor Transport Method for AOM and Radiation Detection Applications," *J. Crystal Growth*, **450**, 96-102(2016).
22. Shi, Y., Yang, J. F., Liu, H., Dai, P., Liu, B., Jin, Z., Qiao, G. and Li, H., "Fabrication and Mechanism of 6H-type Silicon Carbide Whiskers by Physical Vapor Transport Technique," *J. Crystal Growth*, **349**, 68-74(2012).
23. Fanton, M. A., Li, Q., Polyakov, A. Y., Skowronski, M., Cavalero, R. and Ray, R., "Effects of Hydrogen on the Properties of SiC Crystals Grown by Physical Vapor Transport: Thermodynamic Considerations and Experimental Results," *J. Crystal Growth,* **287**, 339-343(2006).
24. Paorici, C., Razzetti, C., Zha, M., Zanotti, L., Carotenuto, L. and Ceglia, M., "Physical Vapour Transport of Urotropine: One-Dimensional Model," *Mater. Chem. and Phys.*, **66**, 132-137(2000).
25. Rosenberger, F. and Müller, G., "Interfacial Transport in Crystal Growth, a Parameter Comparison of Convective Effects," *J. Crystal Growth*, **65**, 91-104(1983).
26. Markham, B. L. and Rosenberger, F., "Velocity and Concentration Distribution in a Stefan Diffusion Tube," *Chem. Eng. Commun.,* **5**, 287-298(1980).
27. Bird, R. B., Stewart, W. E. and Lightfoot, E. N., *Transport Phenomena*, John Wiley and Sons, New York, NY(1960).
28. Reid, R. C., Prausnitz, J. M. and Poling, B. E., *The Properties of Gases & Liquids*, 4th ed., McGraw-Hill, New York, NY(1987).
29. Oppermann, H., "Chemical Aspects of Hg_2X_2-Decomposition, Barogram-Diagram and Thermodynamic Data," Proceedings of the 2nd Int'l Symposium on Univalent Mercury Halides, Czechoslovakia(1989).
30. Weaver, J. A. and Viskanta, R., "Natural Convection due to Horizontal Temperature and Concentration Gradients-1. Variable Thermophysical Property Effects," *Int. J. Heat Mass Transfer*, **34**, 3107-3120(1991).
31. Patankar, S. V., *Numerical Heat Transfer and Fluid Flow*, Hemisphere Publishing Corp., Washington D. C.(1980).
32. Catton, I., "Effect of Wall Conducting on the Stability of a Fluid in a Rectangular Region Heated from Below," *J. Heat Transfer,* **94**, 446-452(1974).
33. Nadarajah, A., Rosenberger, F. and Alexander, J., "Effects of Buoyancy-Driven Flow and Thermal Boundary Conditions on Physical Vapor Transport," *J. Crystal Growth,* **118**, 49-59(1992).

34. Kim, G. T. and Kwon, M. H., "Effects of Solutally Dominant Convection on Physical Vapor Transport for a Mixture of Hg_2Br_2 and Br_2 under Microgravity Environments," *Korean Chem. Eng. Res.*, **52**, 75-80(2014).

35. Singh, N. B., Gottlieb, M., Hopkins, R. H., Mazelsky, R., Duval, W. M. B. and Glicksman, M. E., "Physical Vapor Transport Growth of Mercurous Chloride Crystals," *Prog. Crystal Growth and Charact.*, **27**, 201-231(1993).